Percolation, phase separation, and gelation in fluids and mixtures of spheres and rods

Ryan Jadrich and Kenneth S. Schweizer

Citation: The Journal of Chemical Physics **135**, 234902 (2011); doi: 10.1063/1.3669649
View online: http://dx.doi.org/10.1063/1.3669649
View Table of Contents: http://scitation.aip.org/content/aip/journal/jcp/135/23?ver=pdfcov
Published by the AIP Publishing

Percolation, phase separation, and gelation in fluids and mixtures of spheres and rods

Ryan Jadrich[1,2] and Kenneth S. Schweizer[1,2,3,a)]
[1]*Department of Chemistry, University of Illinois, Urbana, Illinois 61801, USA*
[2]*Frederick Seitz Materials Research Laboratory, University of Illinois, Urbana, Illinois 61801, USA*
[3]*Department of Materials Science, University of Illinois, Urbana, Illinois 61801, USA*

(Received 16 September 2011; accepted 21 November 2011; published online 21 December 2011)

The relationship between kinetic arrest, connectivity percolation, structure and phase separation in protein, nanoparticle, and colloidal suspensions is a rich and complex problem. Using a combination of integral equation theory, connectivity percolation methods, naïve mode coupling theory, and the activated dynamics nonlinear Langevin equation approach, we study this problem for isotropic one-component fluids of spheres and variable aspect ratio rigid rods, and also percolation in rod-sphere mixtures. The key control parameters are interparticle attraction strength and its (short) spatial range, total packing fraction, and mixture composition. For spherical particles, formation of a homogeneous one-phase kinetically stable and percolated physical gel is predicted to be possible, but depends on non-universal factors. On the other hand, the dynamic crossover to activated dynamics and physical bond formation, which signals discrete cluster formation below the percolation threshold, almost always occurs in the one phase region. Rods more easily gel in the homogeneous isotropic regime, but whether a percolation or kinetic arrest boundary is reached first upon increasing interparticle attraction depends sensitively on packing fraction, rod aspect ratio and attraction range. Overall, the connectivity percolation threshold is much more sensitive to attraction range than either the kinetic arrest or phase separation boundaries. Our results appear to be qualitatively consistent with recent experiments on polymer-colloid depletion systems and brush mediated attractive nanoparticle suspensions. © *2011 American Institute of Physics*. [doi:10.1063/1.3669649]

I. INTRODUCTION

Kinetically arrested nanoparticle and colloid states can endow unique and useful material properties to complex fluids, including soft solid-like elasticity and stress-driven yielding response.[1–3] For example, the direct write printing of durable conductive electrodes for solar microcell applications employ metallic nanoparticles in both the fluid and gel states and necessitates careful tailoring of structure, electrical transport, and mechanical properties.[4] Macroscopic amorphous solidity and conductivity requires both kinetic arrest on the relevant time scales and mechanical connectivity percolation. The study of geometric percolation, both site and bond, has a long history based on lattice models.[5,6] Continuum percolation is less understood due to the inherent structural disorder and ambiguity of defining a connectivity bond in physical (not chemical) gels. Many continuum percolation studies have employed liquid state theory methods for attractive spheres.[7–12] More recently, flexible and rigid macromolecules have been studied[13–16] based on the polymer reference interaction site model (PRISM) integral equation theory,[17] an extension of the connectedness Ornstein-Zernike (OZ) integral equation theory[10,11,18] for spherical particles.

Connectivity percolation is a necessary, but not sufficient, condition to form a kinetically stable space spanning solid. Local rigidity is also required, corresponding to long lived "physical bonds" for gelling fluids. Indeed, true kinetic arrest requires, at a minimum, connectivity percolation *and* the lifetime of local particle arrangements to exceed the experimental time scale of interest. There is a large literature on the local dynamics aspect for spherical particles (glasses and gels) based on the microscopic ideal mode-coupling theory (MCT) approach,[19] which predicts a dynamic crossover from fast liquid-like dynamics to transient localization and slow collective structural relaxation. However, the long time dynamical arrest transition predicted by ideal MCT is avoided via ergodicity-restoring rare activated barrier hopping processes in both glasses and gels. An extensively developed microscopic approach to describe single particle, ergodicity-restoring hopping, for both spheres and non-spherical rigid particles, is the nonlinear Langevin equation (NLE) theory.[20–24] Both MCT and NLE theories focus on local kinetic arrest, and the connection between structure, interactions and slow dynamics. At a minimum, theoretical estimation of the emergence of global rigidity requires combining such local dynamical theories with a percolation analysis.

At zeroth order, two types of kinetically arrested states are predicted for spheres: glasses and gels.[19,25–31] Vitrification is driven by repulsive forces at high concentrations, while gelation is triggered by physical bond formation. Gels have been diversely described as a consequence of local stickiness plus bond percolation in a homogeneous phase, or via coupling to spatially inhomogeneous processes such as crystallization, spinodal phase separation into dense percolating particle domains, or diffusion limited cluster aggregation of

a)Electronic mail: kschweiz@illinois.edu.

fractal or compact clusters formed either kinetically or via a nucleation and growth mechanism.[25–27,32] A full understanding of these issues, and the degree of universality of physical gelation, is rather poor, especially for non-spherical particle fluids.

In addition to nonequilibrium phase behavior and mechanical properties, understanding the interplay between percolation, kinetic arrest and phase separation is an important topic for materials science applications such as creating conducting and/or processable/printable nanoparticle gels.[4,33] The design rules for material selection (particle size and shape, intermolecular forces) and thermodynamic state (volume fraction, mixture composition, temperature) to controllably shift the absolute and relative location of phase separation, percolation, dynamic crossover and kinetic vitrification boundaries is a problem of broad relevance. This paper reports our initial theoretical efforts in this direction based on applying a combination of statistical mechanical methods.

Section II summarizes the models and theories employed. Equilibrium pair structure, which is the critical input to the percolation, phase separation and dynamical theories, is briefly addressed in Sec. III. Section IV studies the connectivity percolation of pure rod and sphere fluids, and their mixtures. The onset of transient localization and activated dynamics, and true kinetic arrest, is studied in Sec. V for sphere fluids. The relation between local dynamical arrest, percolation and phase separation is investigated, and comparison with both experiments and computer simulations on particle gels presented. Section VI addresses the same theoretical questions as in Sec. V for rods of two very different aspect ratios. The paper concludes in Sec. VII with a summary and discussion.

II. THEORY

We employ a suite of existing theoretical methods, equilibrium and dynamic. Only the essential elements relevant to our present work are summarized since detailed discussions can be found in the literature.

A. Particle models and structural correlations

We consider fluids of spheres, and rigid rods composed of tangent spherical interaction sites, where all sites interact via a pair potential consisting of a hard core plus square well attraction

$$v(r) = \begin{cases} \infty, & r < \sigma \\ -\varepsilon, & \sigma < r < \sigma + a \\ 0, & \sigma + a < r \end{cases}. \quad (1)$$

Here, σ is the hard core diameter of spherical sites (taken as the unit of length), and a and ε the contact attraction range and strength, respectively. For both simplicity and our desire to mimic chemistry-matched systems of practical interest (e.g., silver nanoparticle systems[4,33]), all sites are chosen to have the same σ, ε (reported in units of the thermal energy, k_BT), and spatial range; this restriction is readily lifted. A square well attraction is employed since it allows a natural choice of connectivity distance for sticky particle fluids. Here, we study two cases relevant to short range attractions of various origins[1] in nanoparticle and colloid suspensions: $\Delta = a/d = 0.02$ or 0.08.

Site-site pair correlation functions are computed using integral equation theories, the reference interaction site model (RISM)[34] for multi-site objects, or the standard OZ equation[18] for spheres

$$\boldsymbol{H}(k) = \Omega(k)\boldsymbol{C}(k)[\Omega(k) + \boldsymbol{H}(k)]. \quad (2)$$

Here, the matrices $\boldsymbol{H}(k)$ and $\boldsymbol{C}(k)$ contain the Fourier transforms of $\rho_i\rho_j h_{ij}(r)$ and the direct correlation function $C_{ij}(r)$, respectively, $h_{ij}(r) = g_{ij}(r) - 1$, where $g_{ij}(r)$ is the radial distribution function, $\boldsymbol{\Omega}(k)$ is a diagonal matrix containing the density-weighted Fourier transformed intramolecular structure factors, $\rho_i\omega_i(k)$, that describe particle shape, where ρ_i is the site number density of species i. Subscript "s" indicates spheres and "r" indicates rods. For rods, end effects are preaveraged in the standard manner corresponding to an equivalent site approximation.[17]

For a sphere, $\omega_s(k) = 1$, while for a rod composed of N tangent sites,

$$\omega_r(k) = \frac{1}{N}\sum_{\alpha,\beta=1}^{N} \frac{\sin(r_{\alpha\beta}k)}{r_{\alpha\beta}k}, \quad (3)$$

where $r_{\alpha\beta} = |\alpha - \beta|\sigma$. The Percus-Yevick (PY) closure approximation is employed[34]

$$\begin{aligned} C_{ij}(r) &= (e^{\beta v(r)} - 1)g_{ij}(r), \quad r > \sigma, \\ g_{ij}(r) &= 0, \quad r < \sigma. \end{aligned} \quad (4)$$

The integral equations are numerically solved using either the Picard or Newton-Raphson algorithm.[18] Knowledge of the pair correlation functions allows computation of the number of sticky connections (n_{ij}) experienced by a tagged particle of type i with particles of type j as

$$n_{ij} = N_i \int_{\sigma}^{\sigma+a} dr 4\pi r^2 \rho_j g_{ij}(r), \quad (5)$$

where N_i is the number of sites of a particle of type i. For s-s connections, Eq. (5) is the mean number of "connected" neighbors of a tagged sphere. However, for r-r connections it is the number of connected sites on all rods surrounding a tagged rod. The dimensionless site-site collective partial (scattering) structure factors are given by

$$S_{ij}(k) = \delta_{ij}\omega_i(k) + \sqrt{\rho_i\rho_j}h_{ij}(k). \quad (6)$$

Macroscopic spinodal phase separation corresponds to the condition: $S_{ij}(k=0) \to \infty$. For a rod fluid, the center-of-mass (CM) structure factor and direct correlation function follow from the site level information as:[22]

$$S_{CM}(k) \cong \frac{S_{rr}(k)}{\omega_r(k)}, \quad (7)$$

$$C_{CM}(k) \cong N\omega_r(k)C_{rr}(k). \quad (8)$$

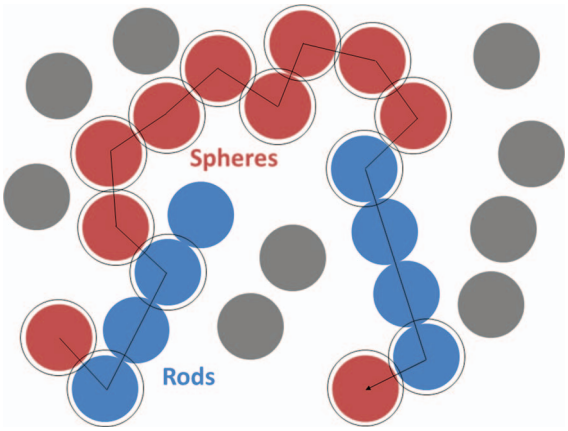

FIG. 1. Schematic of percolation in a binary rod-sphere mixture. The connected distance around a site is denoted by a sphere encapsulating the site and is chosen as the range of attraction. A percolating pathway is denoted by an arrow.

B. Connectedness RISM and percolation

A connectivity distance must be defined between a pair of interaction sites. We employ the square well attraction range, i.e., connectivity is identified with physical bond formation. The relation analogous to Eq. (2) for the percolation problem[7–16]

$$H^+(k) = \Omega(k)\boldsymbol{C}^+(k)[\Omega(k) + \boldsymbol{H}^+(k)], \tag{9}$$

where $\boldsymbol{H}^+(k)$ and $\boldsymbol{C}^+(k)$ are equivalent to the standard liquid theory analogs except they only account for pairs of particles that are connected via a percolating pathway of intermediate particles, as shown in Fig. 1. Equation (9) is closed by the analogous connectedness PY approximation

$$\begin{aligned} h_{ij}^+(r) &= g_{ij}^+(r) = g_{ij}(r), \quad r < (\sigma + a), \\ C_{ij}^+(r) &= 0, \quad r > a, \end{aligned} \tag{10}$$

where $g_{ij}^+(r) = h_{ij}^+(r)$ is the connectedness analog of $g_{ij}(r)$. Physically, $g_{ij}^+(r)$ is proportional to the probability that there is another particle at a distance r away from a tagged particle that is connected by a percolating pathway.

The total number of sites in a connected cluster for the sphere-rod mixture is given by

$$\begin{aligned} S_{total}^+(k=0) = \Phi_s S_{ss}^+(k=0) + \sqrt{\Phi_s \Phi_r} S_{sr}^+(k=0) \\ + \Phi_r S_{rr}^+(k=0), \end{aligned} \tag{11}$$

$$S_{ij}^+(k) = \delta_{ij}\omega_i(k) + \sqrt{\rho_i \rho_j} h_{ij}^+(k), \tag{12}$$

where Φ_i is the fraction of the total site level packing fraction, η, composed of particle sites of species i (spheres or rods). The divergence of $S_{total}^+(k=0)$ signals the emergence of a macroscopic connected cluster, i.e., the percolation threshold.

C. Naïve MCT and NLE theory

For studying the dynamical crossover (ideal MCT transition) and activated hopping regime, we employ the center-of-mass versions of naïve mode coupling theory (NMCT) and NLE theory, respectively. The CM approximation for rods corresponds to no dynamical rotation.[22] This greatly simplifies the technical complexity of the theories, and has been shown to be reliable for translational dynamics and the onset of kinetic arrest in a manner that becomes increasingly accurate as rod aspect ratio grows.[24] The dynamic order parameter is the CM scalar displacement of a tagged particle from its initial position, $r(t)$, which obeys a nonlinear stochastic Langevin equation in the overdamped limit[20,22,35]

$$\zeta_S \frac{dr(t)}{dt} = -\frac{\partial F_{dyn}(r(t))}{\partial r(t)} + \delta f(t), \tag{13}$$

where ζ_S is the short time friction constant and the random thermal noise term satisfies $\langle \delta f(0)\delta f(t)\rangle = 2k_B T\zeta_S \delta(t)$. The key quantity is the dynamic free energy, $F_{dyn}(r)$, the derivative of which characterizes the effective force felt by a tagged particle due to all surrounding particles, and in units of $k_B T$ is given by

$$\begin{aligned} F_{dyn}(r) = -3\ln(r) + \int \frac{d\vec{k}}{(2\pi)^3} \frac{\rho C_{CM}^2(k) S_{CM}(k)}{1 + S_{CM}^{-1}(k)} \\ \times \exp\left\{ \frac{-k^2 r^2}{6} \left(1 + S_{CM}^{-1}(k)\right) \right\}. \end{aligned} \tag{14}$$

In the absence of noise (no barrier hopping allowed), Eq. (13) reduces to the naïve MCT (Refs. 20, 22, and 35) self-consistent equation for the CM localization length or long time limit of the mean square displacement $\langle r^2(t \to \infty)\rangle = r_{LOC}^2$

$$\begin{aligned} r_{LOC}^{-2} = \frac{1}{9} \int \frac{d\vec{k}}{(2\pi)^3} \rho k^2 C_{CM}^2(k) S_{CM}(k) \\ \times \exp\left\{ \frac{-k^2 r_{LOC}^2}{6} \left(1 + S_{CM}^{-1}(k)\right) \right\}. \end{aligned} \tag{15}$$

The first occurrence of a finite r_{LOC} solution to Eq. (15) corresponds to the emergence of a dynamic free energy characterized by a localization well and activation barrier (height F_B) located at a displacement r_B. Glasses form via repulsive force caging and are characterized by a "large" localization length (of order a tenth of a particle diameter) and barrier location at $r_B \sim 0.3$–0.4. Gels are generically characterized by a "short" localization length (of order or smaller than the attraction range) due to physical bond formation, with the barrier also typically occurring at small displacements. So-called attractive glasses[25–29] exhibit a short gel-like r_{LOC} and a large-glass-like r_B since both caging and bond formation are relevant to activated dynamics.[23,36,37]

We emphasize that the NMCT glass and gel "transitions" are dynamic crossovers. In the laboratory, kinetic arrest occurs when a relaxation time exceeds the experimental time scale. Here, we compute mean barrier hopping times as a useful surrogate for the particle scale alpha relaxation time[21]

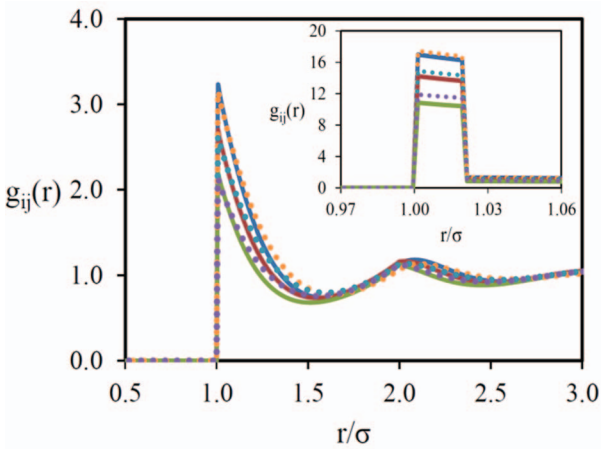

FIG. 2. Site-site radial distribution functions in a rod-sphere mixture for (from top to bottom) sphere-sphere (dark blue and orange), sphere-rod (red and teal), and rod-rod (green and purple) pair correlations. Rods have 5 sites, $\eta = 0.4$, and $\beta\varepsilon = 0$ (athermal limit) in the main plot, and $\beta\varepsilon = 2.5$ with $\Delta = 0.02$ in the inset. Solid curves represent a 20% rod mixture and the dotted curves a 80% rod mixture.

based on Kramers theory:[20,38]

$$\frac{\tau_{hop}}{\tau_0} = \frac{2\pi G}{\sqrt{K_0 K_B}} e^{F_B/k_B T}, \tag{16}$$

where $\tau_0 = N\sigma^2\zeta_0/k_BT$, ζ_0 is the dilute limit particle (site) friction constant, K_0 and K_B are the absolute magnitudes of the curvatures (units of k_BT/σ) at the minimum and barrier of $F_{dyn}(r)$, respectively, and $G = \zeta_S/\zeta_0 = g_{ss}(\sigma)$ is the ratio of the short time friction to solvent friction computed based on a binary collision perspective.[20,39]

III. EQUILIBRIUM PAIR STRUCTURE

Our calculations of the percolation threshold, spinodal demixing boundary, dynamic crossover curves, and kinetic arrest boundary all require the pair structure as input. Here, we present just two examples in Fig. 2 for a 5-site rod-sphere mixture at a fixed total packing fraction of $\eta = 0.4$. Recall that "matched chemistry" conditions have been adopted, i.e., equal attraction strengths and ranges and site diameters for all species. We have verified that this condition results in small variations of pair structure with mixture composition. The main frame of Fig. 2 shows the insensitivity under purely hard core conditions. Varying composition from 20% to 80% rods does not significantly change the three site-site pair correlations.

The inset of Fig. 2 shows the near contact region for a strongly attractive system with $\varepsilon = 2.5$. The high contact peak signifies strong local clustering, which aids percolation. Based on Eq. (5), the total number of sticky connections (n_i^{total}) experienced by a tagged particle is given by $n_i^{total} = \sum_{j=r,s} n_{ij}$. This yields for the 20% rods in Fig. 2, $n_s^{total} = 3.15$ and $n_r^{total} = 13.0$, and for the 80% rod mixture, $n_s^{total} = 2.96$ and $n_r^{total} = 12.0$. The total number of sticky connections does not change very much with composition, a consequence of the near structural invariance under matched chemistry conditions.

IV. PERCOLATION

There are several characteristic packing fractions for rod fluids. The onset of intermolecular interactions occurs at the "dilute-to-semidilute" crossover:[40] $\eta^* \equiv N(\pi\sigma^3/6)/R_g^3 \propto N^{-2}$, for $N \gg 1$, where R_g is the radius of gyration which for long rods scales as $\sim N\sigma$. For hard long rods, the isotropic-nematic transition occurs at[41] $\eta_{IN} \approx 4/N$. In the present study, we consider only isotropic fluids. Our calculations for a long rod ($N = 40$) are thus relevant at high η only if the nematic phase transition is kinetically avoided. An analogous situation is encountered for hard spheres where glassy dynamics emerges at volume fractions above the equilibrium fluid-crystal phase transition at $\eta \sim 0.495$. Many experiments on long attractive rods do indeed observe isotropic gels, presumably due to kinetic arrest pre-empting liquid crystal formation.[42]

A. Rod-sphere mixtures

Percolation in mixtures depends on a larger parameter space compared to one-component fluids. Here, we study rod-sphere mixtures for two aspect ratios (5 and 40) that experience attractions of variable strength (ε) and fixed dimensionless spatial range of $\Delta = 0.02$.

Percolation diagrams are plotted in Figs. 3 and 4 in the representation of total mixture packing fraction (η) versus rod mixture composition (Φ_R). For all systems studied, we find the percolation threshold occurs in the one phase region. Two distinct percolation boundaries are calculated at a given attraction strength: a "full" percolation boundary that allows for connections between all types of sites, and its "disconnected" analog where sphere-rod connections are not taken into account. Examination of these two boundaries provides insight concerning whether one of the species dominates percolation, and the role of interconnections between spheres and rods.

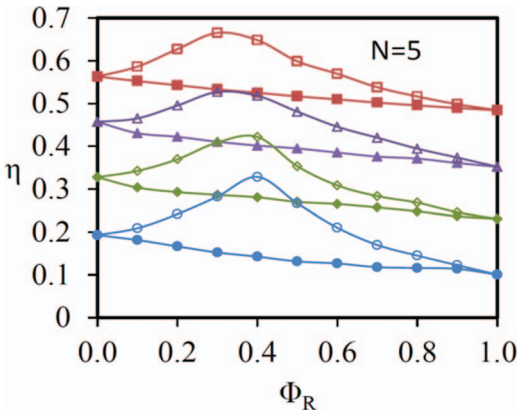

FIG. 3. Fluid total packing fraction at the percolation threshold for a binary mixture of spheres and 5-site rods as a function of the rod volumetric composition at a fixed attraction range of $\Delta = 0.02$. Red squares are results for $\beta\varepsilon = 0$, purple triangles for $\beta\varepsilon = 1$, green diamonds for $\beta\varepsilon = 2$, and blue circles for $\beta\varepsilon = 3$. Open symbols only allow for sphere-sphere or rod-rod connections; closed symbols allow the additional sphere-rod contribution to connectivity.

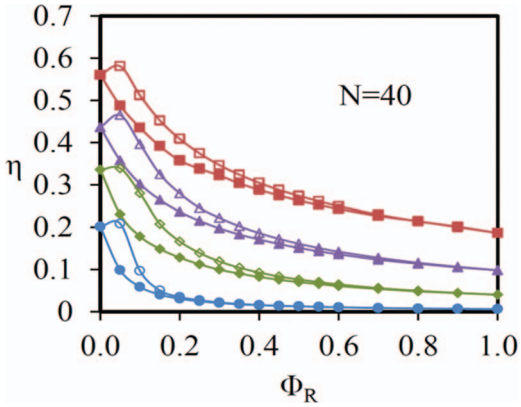

FIG. 4. Same as Fig. 3 but for a 40-site rod.

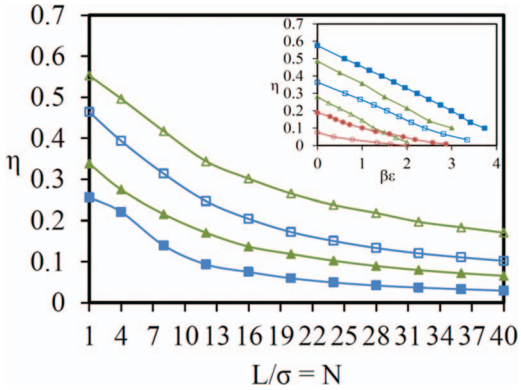

FIG. 5. One-component fluid packing fraction at the percolation threshold as a function of aspect ratio $L/\sigma = N$; green triangles are for $\beta\varepsilon = 0.2$ and blue squares are for$\beta\varepsilon = 1$. Open symbols represent a connectivity distance and attraction range of $\Delta = 0.02$, and closed symbols are for $\Delta = 0.08$. Inset: Attraction strength dependence for spheres (squares), 5-site rods (triangles), and 40-site rods (circles). Closed symbols are for $\Delta = 0.02$ and open symbols for $\Delta = 0.08$.

For both the aspect ratio mixtures, the full percolation boundaries are monotonic functions of rod volume fraction, reflecting the well-known higher percolating power of extended objects compared to spheres.[13,16] However, the disconnected percolation boundary is a non-monotonic function of rod volume fraction, and for all attraction strengths exhibits a maximum at $\Phi_R \approx 0.3$–0.4 for 5-site rods, and $\Phi_R \approx 0.05$ for 40-site rods. The relative insensitivity of the long rod system maximum to attraction strength suggests this feature is largely controlled by geometric factors. The maximum defines a most difficult to percolate state and always occurs when the rods are the minority component. The existence of such a maximum implies that as a small amount of rods displace spheres at fixed packing fraction, more sphere-sphere connections are lost than rod-rod connections are formed, and hence the percolation threshold rises. However, upon addition of enough rods, they begin to directly percolate, and the mixture percolation threshold decreases. Quantitatively, the influence of inter-species connections on percolation increases as the attraction strength grows.

Figures 3 and 4 also illustrate that changing attraction strength does not alter the basic form of the percolation boundaries, but rather only lowers the threshold by a roughly constant increment, roughly linearly with increasing ε. It appears that as attraction strength grows, the relative effect of particle anisotropy on the percolation threshold is magnified. For example, Fig. 3 shows that upon transitioning from a pure sphere to a pure rod fluid the percolation threshold drops by 14% at $\varepsilon = 0$, compared to 48% at $\varepsilon = 3$.

By comparing Figs. 3 and 4, it is evident that adding 40-site rods to a sphere fluid results in larger changes in the percolation threshold than adding 5-site rods. The fully connected curves in Fig. 4 for the longer rod mixture now overlap the "disconnected" analogs for most of parameter space. This strong overlap, which begins at $\Phi_R \approx 0.3$, indicates that only at quite low rod compositions do the spheres significantly participate in the percolation transition. This is in strong contrast to the 5-site rod mixtures in Fig. 3, where the overlap of the connected and disconnected curves is never appreciable. The more pronounced maximum in the disconnected curves for 5-site rod case is further evidence of the rod dominance of the percolation threshold.

Finally, we note that the percolation thresholds are at much higher packing fractions, and are less N-dependent, than the dilute-semidilute threshold which decreases by a factor of 64 as rod length is increased from 5 to 40. However, the sensitivity to N of the percolation packing fraction does become stronger as attraction strength grows.

B. Dependence of rod percolation on aspect ratio and attraction

Figure 5 presents a systematic study of the dependence on aspect ratio of the percolation threshold in *pure* rod fluids at various fixed values of attraction strength and range. The main frame shows results at $\varepsilon = 0.2$ and 1 for the two standard dimensionless ranges of $\Delta = 0.02$ and 0.08. For aspect ratios greater than ~10, the percolation volume fractions follows an apparent inverse power law: at $\varepsilon = 0.2$, $\eta_{perc} \sim N^{-0.57}$ and $N^{-0.76}$ for $\Delta = 0.02$ and 0.08, respectively, while at $\varepsilon = 1$, $\eta_{perc} \sim N^{-0.78}$ and $N^{-0.95}$. Evidently, increasing the attraction range enhances the dependence of the percolation threshold on aspect ratio. For $\varepsilon = 1$ and $\Delta = 0.08$, the N dependence is almost as strong as the N^{-1} scaling of the isotropic-to-nematic phase transition volume fraction. Fixing the attraction range, and increasing the attraction strength results in a stronger N-dependence of the percolation threshold due to the enhanced local packing or clustering of rods.

As expected, the attraction range also has a large effect on the absolute value of the percolation thresholds which decrease dramatically as the range grows from 0.02 to 0.08. This decrease is similar for $\varepsilon = 0.2$ and $\varepsilon = 1$, but the relative reduction is much larger for the more attractive system due to the enhanced number of sticky contacts.

The detailed dependence of the percolation threshold on attraction strength is shown in the inset of Fig. 5. A nearly linear variation occurs until high attraction strengths are reached. Linearity persists longer for smaller aspect ratios and shorter attraction ranges. Deviations in linearity are observed for 40-site rods, presumably because it is a highly interpenetrating fractal object.

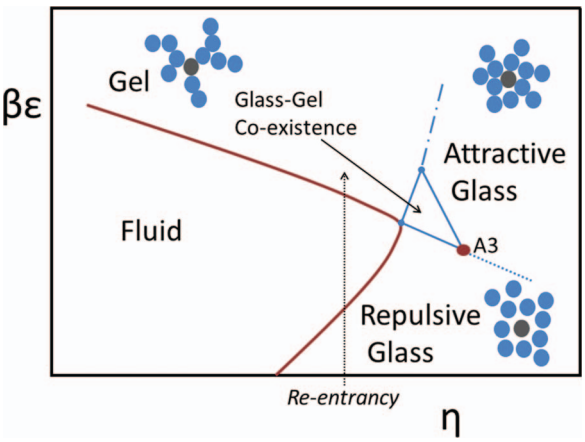

FIG. 6. A qualitatively correct schematic kinetic arrest diagram for spheres and rods at the CM level.[23] Distinct dynamically arrested states are gels, attractive glasses, repulsive glasses, and the glass-gel "coexistence" regime. The A3 point signals termination of the ability to distinguish repulsive and attractive glasses based on their localization length.[25–28] The dashed lines beyond the A3 point is a more fuzzy crossover boundary indicating a rapid, but smooth, change from glass-like to gel-like localization.[23] The heavy red solid curve surrounding the fluid regime indicates the initial fluid-to-solid ideal transition or dynamic crossover. Sketches of particle arrangements in various states are shown. The vertical arrow indicates a sample re-entrancy trajectory for a repulsive glass → fluid → gel transition.

V. KINETIC ARREST, PERCOLATION, AND DEMIXING OF SPHERES: MODEL CALCULATIONS AND COMPARISON TO EXPERIMENT AND SIMULATION

A. Dynamics background

NMCT is a mathematically and conceptually simplified single particle version of the full ideal MCT for collective density fluctuations.[20] It faithfully captures the dynamic crossover in one-component sphere fluids,[20] partial localization in biphasic mixtures,[39] non-monotonic variation of the kinetic arrest volume fraction with aspect ratio in hard diatomic fluids,[22,24] the possibility of plastic glasses,[24] and other more exotic kinetically arrested states in non-spherical particle systems.[23,24] As relevant background, a typical kinetic arrest diagram for spheres based on NMCT and NLE theory is sketched in Fig. 6; the topology is qualitatively the same for rods at the CM level.[23] By combining NMCT and NLE theories, four distinct dynamically arrested states are predicted:[23,24] repulsive glass (RG), gel (G), attractive glass (AG), and a glass-gel (GG) "co-existence" region. In NLE theory, crossing a NMCT boundary results in a dynamic free energy that exhibits a localized state and activation barrier. In the present work, only the initial kinetic arrest boundary will be shown (indicated by the bold red curve in Fig. 6). The non-monotonic "nose" feature signals a re-entrancy transition from RG → fluid(F) → G associated with a change from repulsive force caging to attractive force bond formation as the primary mechanism for transient localization.[23,26–29] The dynamic crossover boundaries are not unambiguously determinable in experiment or simulation, where "arrest" is defined via a kinetic criterion related to a chosen time scale, identified here with the mean barrier hopping time.

Since both MCT and NLE theories describe local arrest, identification of global gelation requires additional knowledge about percolation and connectivity. We compare the theoretical (local) kinetic arrest boundaries with our computed percolation thresholds, and identify global arrest when the system is beyond *both* the boundaries, which we interpret as a kinetically stable connected network. An important question is when this global arrest boundary intersects the liquid-liquid phase separation spinodal, which heralds the beginning of gelation triggered by macrophase separation. If percolation occurs before the ideal NMCT boundary is encountered, then one does not even expect dynamically arrested clusters to be present. On the other hand, if the NMCT boundary is crossed before the percolation boundary, then a regime exists where finite-sized clusters of physically bonded particles likely exist.

As a general caveat, we emphasize the irrelevance of the percolation line to kinetic arrest under weak attraction conditions where gels are not expected, the extreme case being athermal ($\varepsilon = 0$) glass states.

B. Contacts and percolation

As a relevant prelude, we have computed the number of sticky contacts using Eq. (5) in the pure rod and pure sphere fluids *along* the percolation threshold boundaries for a dimensionless attraction range of $\Delta = 0.02$ corresponding to the systems studied dynamically in Figs. 7 and 9, and 10(a). Interestingly, the number of sticky contacts is almost constant. For spheres [Fig. 7(a)], the number of sticky contacts is ∼1.9, very close to the value of 2 required to be exceeded in order that connected branched networks form. For 5-site rods [Fig. 9(a)], we find a tagged rod has ∼3.75 sticky contacts, while for a 40-site rod [Fig. 10(a)] ∼3.4 contacts along the percolation boundary. Whether this near constancy along the pure systems percolation boundary is fortuitous is unclear, but is physically appealing. We note there are successful heuristic models of the percolation threshold based solely on the usual pair correlation functions, $g_{ij}(r)$ not $g_{ij}^{+}(r)$, and a critical number of connected nearest neighbors criterion.[43] Results from one such theory agree extremely well with computer simulations.[44]

C. Model calculations

Figure 7 presents our dynamical results for spheres. The NMCT ideal kinetic arrest (dynamic crossover) boundaries exhibit the well known nose and re-entrancy features at high packing fractions as attraction strength is varied, which becomes less pronounced with increasing attraction range.[28,29] The percolation threshold and spinodal phase separation boundary are overlaid. For both attraction ranges, the dynamic crossover occurs well below the spinodal demixing curve for packing fractions above the critical point. For the short range attraction system, the percolation threshold crosses the NMCT boundary at η ∼0.35. Hence, below this packing fraction, a window of attraction strength (or temperature) exists where dynamic clusters or aggregates may be present. Moreover, the dynamic crossover and percolation threshold lie below the demixing spinodal even at low packing fractions below the critical point.

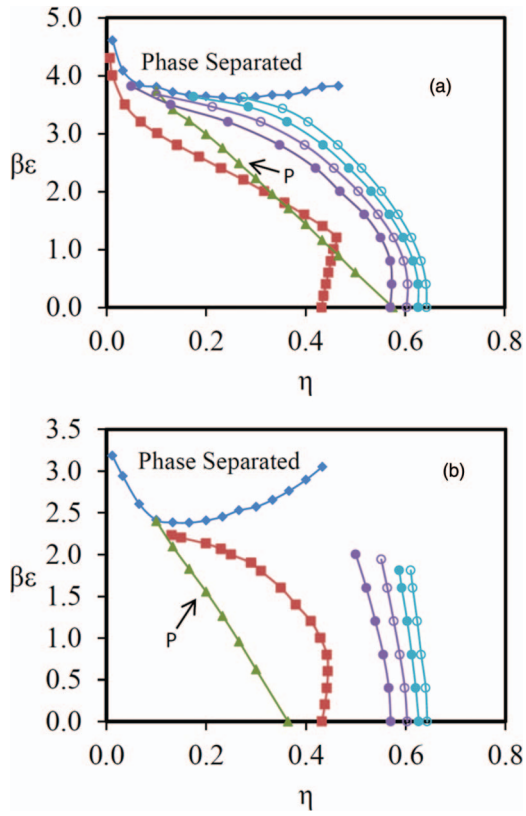

FIG. 7. (a) Mixed dynamic-demixing-percolation phase diagram for sphere fluids with an attraction range of $\Delta = 0.02$. The percolation threshold is represented by the green triangle and is denoted by the symbol "P," the NMCT dynamic crossover boundary by red squares, and the spinodal phase separation boundary by blue diamonds. Circles indicate kinetic arrest boundaries based on activated hopping relaxation time criteria of τ_{hop}/τ_0(bottom to top): 10^2, 10^4, 10^6, and 10^8. (b) Same as (a) but for an attraction range of $\Delta = 0.08$.

There are significant differences for the longer range attractive system in Fig. 7(b). The percolation boundary remains below the dynamical crossover for packing fractions all the way down to the critical point. Moreover, the NMCT boundary is much closer to the demixing curve than for the 2% range system, and both the percolation and dynamic crossover boundaries appear to intersect the spinodal curve just below the critical point.

To address the practically relevant question of arrest into a kinetically stable space-spanning gel, we compute kinetic arrest boundaries using the mean barrier hopping time and a physical criterion for bond lifetime. The mean hopping time in Eq. (16) is expressed in units of the dilute solution (pure solvent for suspensions) Brownian time scale, which for a sphere is $\tau_0 = \sigma^2\zeta_0/k_BT$. For 25 and 100 nm diameter particles (as often studied using silica colloids[45–47]), and a 2 μm particle (typical size of PMMA colloids in confocal experiments[48]), we estimate using a typical solvent viscosity that at room temperature: $\tau_0 \sim 0.15$ ms, 0.01 s, and 30 s, respectively. Confocal microscopy, dynamic light scattering, and rheology experiments correspond to observation times of ~10 to 10 000 s. Four dynamical arrest boundaries are presented in Fig. 7 corresponding to kinetic arrest criteria of $\tau_{hop}/\tau_0 = 10^2$, 10^4, 10^6, and 10^8. In terms of our real world estimates, these correspond to: 0.015, 1.5, 150, and 15 000 s for 25 nm colloids; 1 s, 100 s, 10 000 s, and 11.6 days for 100 nm colloids; and 3000 s, 83 h, ~1 year, and ~1 century for 2 μm colloids.

For the 2% attraction range system [Fig. 7(a)], the kinetic arrest boundaries all occur after percolation, and intersect the spinodal curve at an attraction strength of ~3.5 in the vicinity of the critical point at $\eta \sim 0.23$. Although the flatter binodal demixing curve would lie below the spinodal curve (meeting it at the critical point), our calculations for this short range attraction suggest a gelled network can form in the homogeneous phase over an extended window of packing fractions. For the longer range attractive system [Fig. 7(b)], the critical packing occurs at a lower value of ~0.18. Our more limited (due to numerical convergence of integral equation issues) hopping time calculations suggest that the kinetic arrest curves would intersect the demixing boundary at much high packing fractions, $\eta \sim 0.45$–0.6. Hence, in this case kinetically stable gels likely will not occur in the one phase region.

D. Comparison to experiments

Our calculations are relevant to several recent experiments which have come to different conclusions concerning the question of whether physical gels form in the homogeneous phase.

Zukoski and co-workers[46,47] have carried out extensive studies of the structure (via small angle scattering), gelation and elasticity of polymer-colloid depletion systems based on sterically stabilized (brush-coated) silica spheres of diameter ~50 nm. Depletion attraction ranges of $R_g/R \sim 0.025$–0.09 were studied over a wide range of colloid volume fractions from $\eta \sim 0.15$–0.45. Under repulsive inter-brush (hard sphere) conditions, based on small angle x-ray scattering they found no evidence of fluid-fluid demixing as a precursor of gel formation. Similar conclusions were drawn for the same brush coated particles when temperature was varied to induce direct attractions in the absence of polymer additives, i.e., macrophase demixing is not the origin of the observed gelation. The measured gelation onset and shear modulus of all these silica-based systems were in good agreement with NMCT theory calculations under the assumption that the relevant structure (fully 2-component for the polymer-particle depletion systems) is that of the *homogeneous* phase.[30,46,47] This prior work is broadly consistent with the new calculations in Fig. 7 for the shorter range attraction.

More recently, Lu *et al.*[32] have come to the different conclusion that for a model polymer-colloid depletion system, gelation always occurs in a two-phase region triggered by spinodal decomposition and only finite clusters occur in the homogeneous phase. Simulation support[49] based on effective 1-component models was also provided. There are significant differences in the experimental systems studied compared to the above silica nanoparticle studies.[46,47] The colloids are much larger (~2 μm), although the depletion range is similar ($R_g/R \sim 0.02$, 0.06). The volume fractions studied were rather low, $\eta \sim 0.045$, 0.13, 0.16, which fall below the critical point

at $\eta \sim 0.27$. Nevertheless, these results are not inconsistent with our calculations in Fig. 7 (for a square well, not depletion, attraction) over the rather low volume fraction regime studied.

Very recently, Wagner and co-workers[45] have studied even smaller, brush-coated silica particles (28 nm diameter) where attraction is induced by varying temperature, over a wide range of $\eta \sim 0.095$–0.52. They estimated the attraction range as 1% of the nanoparticle diameter, and performed approximate theoretical calculations of the binodal and percolation threshold curves. Visual observation, small angle neutron scattering, fiber optic quasielastic light scattering, and rheology were employed to probe this system. Their conclusion was that over a wide range of volume fractions, gelation does occur in a one phase region, not triggered by phase separation, in accord with the prior studies of Zukoski and co-workers[46,47] At volume fractions above the critical point, the kinetic gel line was found to be close to the theoretically estimated percolation boundary if the volume fraction is not too large. At zeroth order, these results seem qualitatively consistent with our calculations for a 2% attraction range in Fig. 7(a).

At a more quantitative level, the new silica nanoparticle study[45] estimated the attraction strength (based on a square well, not depletion, potential) at gelation varies from ~4.5 at a volume fraction of ~0.2, to ~2 at a volume fraction of ~0.45. Although we do not wish to overemphasize precise numerical comparisons given the approximate nature of our model and theory (and real world complications), it seems these numbers are in reasonable accord with our results in Fig. 7(a). We also note that the rheological characterization employed a frequency, which, for a 25 nm particle, corresponds to our kinetic gelation criterion of roughly $\tau_{hop}/\tau_0 = 10\,000$. The calculations in Fig. 7(a) based on the later criterion appear consistent with experiment. The rheology measurements showed a storage modulus that tends to turn down at the lowest frequencies probed, even in a putative gel state. We believe this implies the existence of a finite alpha relaxation time associated with the thermally activated bond breaking, consistent with the NLE theory.[21,31]

E. Comparison to simulations

Our conclusions concerning whether kinetic gelation occurs in the one phase region are obviously sensitive to the quantitative accuracy of the various approximate theories employed for the absolute, and especially relative, location of equilibrium and dynamic phase boundaries. In this section, we address this issue by comparing with relevant simulation results for the square well fluid, and also the adhesive hard sphere (AHS) fluid as a limiting model. A key issue is how equilibrium properties (spinodal and percolation boundaries) scale with attraction range compared to the ideal MCT crossover and kinetically defined activated hopping arrest boundaries. The experiments of Lu *et al.*[32] were interpreted as confirmation of a proposed simulation-based proof[49] that, except at very high volume fractions, gelation can only occur in a 2-phase region. Clearly, the conflicting experimental

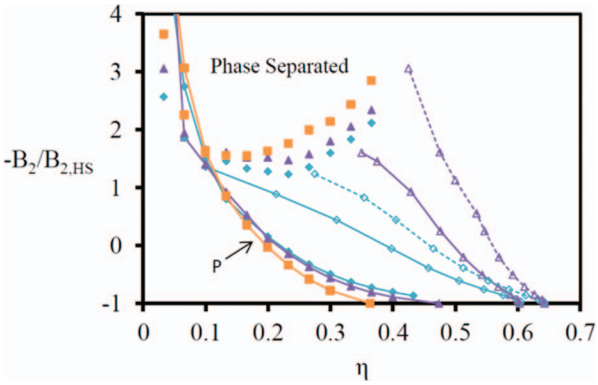

FIG. 8. Mixed dynamic-demixing-percolation phase diagram for sphere fluids plotted in terms of the reduced second virial coefficient as a measure of attraction strength. Teal diamonds are for $\Delta = 0.02$, purple triangles for $\Delta = 0.04$, and orange squares for $\Delta = 0.08$. Spinodal boundaries are denoted only by filled points and percolation boundaries with smooth curves. Hopping time criterion boundaries for $\tau_{hop}/\tau_0 = 10^4$ (solid line) and 10^8 (dashed line) appear as open symbols.

conclusions of Refs. 32, 45, and 46 establish the subtle nonuniversal nature of this question independent of the accuracy of theories.

We first discuss equilibrium boundaries. Several computer simulations of the square well fluid have found that when the range of interaction is very small a universal behavior emerges for the spinodal demixing and percolation boundaries that is closely tied to the limiting AHS model.[50–53] The key parameter is the second virial coefficient normalized by its hard sphere limit, $B_2/B_{2,HS} = 1 - (e^{\beta\varepsilon} - 1)([1 + \Delta]^3 - 1)$. This quantity is negative for strong attractions, and for $\beta\varepsilon \gg 1$ and $\Delta \ll 1$ becomes $B_2/B_{2,HS} \to -3\Delta e^{\beta\varepsilon}$. An important consequence is that the spinodal and percolation boundaries of systems with different (but very short) attraction ranges and strengths can each be collapsed in this reduced second virial coefficient representation.[51]

In Fig. 8, we present representative calculations of the spinodal and percolation boundaries plotted in the reduced B_2-format for three attractions ranges of interest to us: $\Delta = 0.02, 0.04, 0.08$. The percolation boundaries collapse well (better with decreasing range), and are in reasonable accord with AHS simulations (not shown), a well-known fact based on the exact Baxter solution using the PY closure.[53] One also sees a near collapse of the spinodal curves, which have been determined via numerical extrapolation using the compressibility route to the thermodynamics. At $\Delta = 0.02$, we find the critical point is at $\eta_c \sim 0.25$ and the reduced $B_2 \sim -1.15$, which can be semi-quantitatively compared to AHS simulation[50] results of $\eta_c \sim 0.12$ and reduced $B_2 \sim -1.6$. For $\Delta = 0.08$, we find $\eta_c \sim 0.18$ and reduced $B_2 \sim -1.6$, which can be semi-quantitatively compared with $\Delta = 0.15$ square well fluid simulation results of $\eta_c \sim 0.21$ and reduced $B_2 \sim -1.2$.[52]

The dynamic simulations of ultrashort range square well fluids in Ref. 49 focused on $\Delta = 0.01$ and *much lower*. These values are below what we have studied; however, one can still perform qualitative comparisons. Two essential points emerged from the simulations. (1) Ideal MCT is not a good description of the problem for two distinct reasons, especially

because activated hopping events associated with physical bond breaking (not present in ideal MCT) are crucial. This renders any simulation test of our NMCT dynamic crossover curves logically moot, consistent with our view that activated hopping is essential to address using NLE theory. (2) Simulation isodiffusivity curves (a practical estimate, but non-unique, surrogate for a kinetic arrest boundary) were found to collapse well for volume fractions below 0.4 based on the reduced B_2 variable. The physical argument offered for this result was that bond breaking is an activated process, the probability of which scales as the product of an attempt frequency that is inversely proportional to the attraction range times the equilibrium Boltzman factor, i.e., a mean hopping time $\sim\Delta e^{\beta\varepsilon}\propto B_2/B_{2,\,HS}$. Although reasonable as a zeroth order Arrhenius-like argument, it is a highly simplified view given its underlying single bond, gas-like picture. The simulations[49] also found that the isodiffusivity curves intersect the spinodal at volume fractions larger than the critical point. These numerical results and arguments led to the conclusion that for very short range square well attractions the spinodal and kinetic arrest boundaries scale in the same manner with attraction range and strength, and hence gelation in the one phase region cannot occur except at very high volume fractions.

We believe the simulation-based conclusions associated with point (2) above have ambiguities with regards to the essential question of whether it is possible to form kinetic gels in the homogeneous phase. First, the presented isodiffusivity curves and time-dependent functions[49] do not appear to correspond to very slow activated dynamics, at least as traditionally indicated by the following three metrics: a very small diffusion constant $D\lll D_0$ (where D_0 is the bare diffusion constant unaffected by interparticle forces), the presence of near plateaus in the particle mean square displacement, and 2-step relaxation of a local dynamical correlation function. What one means by a gel is intimately tied to these dynamical issues since solidity emerges when the experimental time scale becomes shorter than the equilibrium relaxation time. Hence, it is not possible to unambiguously define a "gelation curve". It also is unclear to us whether the stated finding that the isodiffusivity curves collapse based on the same variable as do equilibrium boundaries is true in a strongly activated (high barrier to bond breaking) regime that is likely relevant to kinetic arrest on experimental time scales.

Microscopic, force-based, approximate dynamic theories that predict an ideal glass or gel transition (MCT, NMCT) do not agree with the idea that the kinetic arrest boundaries scale the same as thermodynamic boundaries.[28,30,54,55] This follows since such dynamical theories are formulated in terms of force-force time correlations, and hence the control parameter for kinetic constraints cannot in general be $\sim\Delta e^{\beta\varepsilon}$. Analysis[54,55] of the square well and related fluids under short range strong attraction conditions suggest the relevant control variable is an effective mean *square* force proportional to $\Delta(e^{\beta\varepsilon}-1)^2$. Of course, the NLE approach argues hopping (or physical bond breakage) is essential and the MCT boundary is only a crossover, but it quantifies dynamical constraints using the same structural information that enters MCT.

Finally, there is the question of the experimentally relevant dynamical arrest boundaries defined via a relaxation time criterion as we have determined based on the NLE theory. Figure 8 shows our theoretical kinetic arrest boundaries do not collapse when plotted in terms of the thermodynamic reduced B_2 variable. Technically, this is not surprising given the discussion in the preceding paragraph, and the fact that NLE theory builds on NMCT in the sense it is formulated in terms of mean square effective forces. Moreover, NLE theory does not generically predict bond breaking barriers are linear in ε and volume-fraction independent,[23,31] a seemingly natural consequence of many body effects on local packing structure and hence the dynamical constraints that determine barriers. Moreover, we have argued above that such a collapse should not be generically expected since kinetic arrest depends on a non-universal relaxation time criterion. Having said that, one sees from Fig. 8 that for the shorter range attractions of 2% and 4%, three out of the four kinetic arrest boundaries do intersect the spinodal curve at packing fractions above the critical point. Indeed, this result is indicative of our main message: whether kinetic gelation via bond formation in the presence of activated hopping processes occurs in a one or two phase region does not have a unique answer even for short range attractive spherical particle fluids. It depends on system details, including the practical experimental issue of what time scale defines the apparent loss of ergodicity or emergence of solidity.

VI. KINETIC ARREST, PERCOLATION, AND DEMIXING: RODS

The behavior of attractive rod fluids is far less studied and understood than its sphere analog. The connection between kinetic arrest, phase separation, and percolation appears to be largely uncharted territory, but is an important topic for the design of new gel-like materials[42] and is also highly relevant in the context of biophysical systems. One expects that strong shape anisotropy modifies both the absolute and relative locations of the various boundaries. The formation of isotropic gels of attractive rod suspensions is ubiquitous in diverse synthetic and biological systems, despite the expectation they may form liquid crystals in equilibrium.[42] In this section, we study the same issues as in Sec. V, but for $N=5$ and 40 rods, where the elementary Brownian time is $\tau_0 = N\beta\zeta_0\sigma^2$.

A. Five-site rods

Figure 9 shows results for 5-site rods. Compared to the sphere behavior in Fig. 7, the onset of slow dynamics (NMCT boundary) shifts further below the spinodal demixing boundary. Note these rods have a critical point at a much lower η than spheres, but a nearly identical critical temperature, as qualitatively expected based on the Flory-Huggins theory of polymer-solvent phase separation.[56] The NMCT dynamic crossover and percolation boundaries intersect at a much lower packing fraction than for spheres, and farther below the critical point for the longer range attractive rod system. The dynamic arrest boundaries based on the relaxation time criteria are also all further below the spinodal curve than found for spheres. For the short attraction range case, forma-

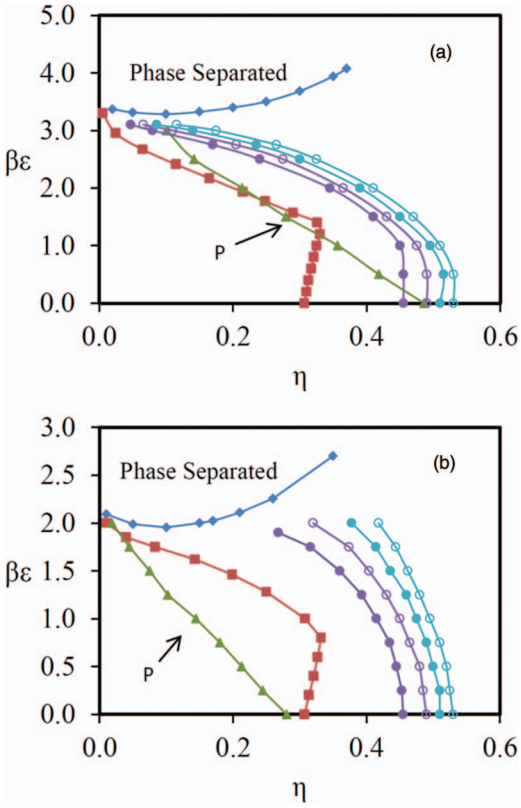

FIG. 9. (a) Same as Fig. 7(a) but for a $N = 5$ site rod with an attraction range of $\Delta = 0.02$. (b) Same as Fig. 9(a) but for an attraction range of $\Delta = 0.08$.

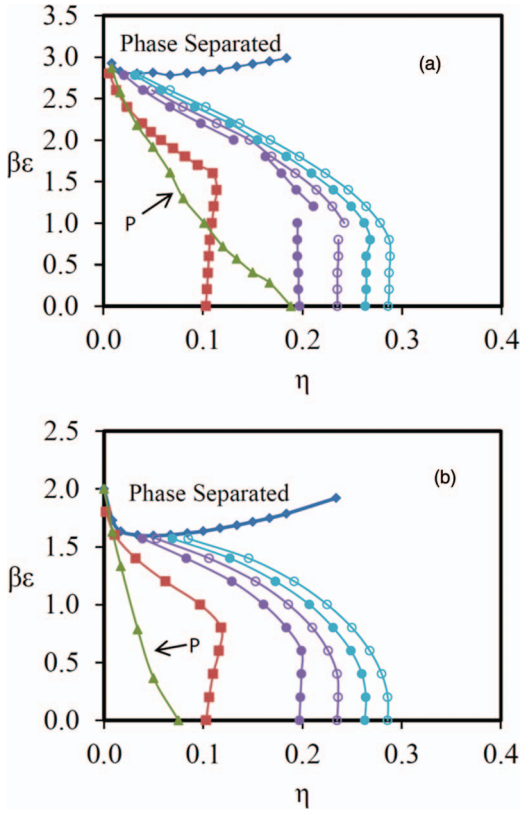

FIG. 10. (a) Same as Fig. 7(a) but for a 40-site rod and an attraction range of $\Delta = 0.02$. (b) Same as Fig. 10(a) but for an attraction range of $\Delta = 0.08$.

tion of a dynamically stable gel network seems rather easy to achieve at packing fractions above the critical point. Increasing the attraction range $\Delta = 0.08$ has the same qualitative effect as it did in spheres, with the dynamic arrest boundaries beginning to intersect the spinodal curve, although stable homogeneous gels are far more likely than for spheres. All these trends reflect the different response of the dynamic boundaries relative to the spinodal and percolation boundaries as particle shape anisotropy is introduced.

The NMCT dynamic crossover boundaries display additional distinctive differences compared to the sphere systems. For the latter, the nose feature becomes more pronounced as attractive range decreases (Fig. 7), and for the large attraction range the nose and re-entrancy essentially disappear. In contrast, Fig. 9 shows the nose feature is still present for 5-site rods with longer range attractions. The relative locations of the dynamic crossover and percolation boundaries resemble the sphere case. For example, upon increasing the attraction range from 0.02 to 0.08, the percolation boundary moves inside the dynamic crossover boundary. Percolation is favored before kinetic arrest for longer range attractions, and the converse applies for the shorter attraction range system.

B. Forty site rods

Calculations for $N = 40$ rods are shown in Fig. 10. Note that for hard rods the NMCT crossover occurs at $\eta \sim 0.10$, as previously established,[57] which is essentially identical to the nematic phase transition point. However, as emphasized above, experimentally there are many examples of large aspect ratio, attractive rods kinetically arresting into gels in a globally isotropic microstructure.[42] Presumably this is because strong attractions can lead to rapid and irreversible sticking, thereby kinetically frustrating the rotational motions required to achieve long range orientational order.

The glass-gel "coexistence region" (see Fig. 6 and Ref. 23) is more pronounced for long rods (not shown in Fig. 10). In this region, the dynamic free energy has two localization wells and two barriers, one glass-like and one gel-like.[23] Hence, the applicability of Kramers theory is problematic (though numerical solution of the NLE equation is well defined), and we do not perform calculations in this region, which is why there are "gaps" in some of the dynamic arrest curves in Fig. 10(a).

The enhanced aspect ratio reduces the fluid window enormously compared to the 5-site rods or spheres, and the dynamic crossover curves are even further removed from spinodal phase separation boundary. Figure 10(a) shows a large kinetic gelation region emerges in the homogeneous phase region based on the employed relaxation time criteria. For an attraction range of 0.02, only at very high attractive strengths and low rod concentration gelation is predicted to intersect the spinodal phase separation boundary. For the longer attraction range in Fig. 10(b), a large window for gelation in the homogeneous phase persists. Figure 10 also shows that percolation relative to kinetic arrest becomes much easier for 40 site rods, with relative shifts compared to the 5-site rods for both attraction ranges. Figure 10(b) demonstrates that it is impossible to have cluster formation (NMCT boundary) or a dynamically arrested state without first being percolated

for the longer attraction range system. Overall, large shape anisotropy assists not only connectivity percolation, but also bond formation and kinetically stable gel networks.

VII. SUMMARY AND CONCLUDING REMARKS

We have theoretically explored the relationship between macrophase separation, bond percolation, kinetic cluster formation, and space spanning gelation in short ranged attractive nanoparticle systems. The experimental observations by some workers that gelation is triggered by phase separation in sphere suspensions is consistent with our calculations at low volume fraction under certain conditions, but it is not a universal feature. The physical reason is twofold: (i) physical gelation involves a relaxation time criterion determined by experimental conditions, and (ii) based on our approximate statistical dynamical theories both the dynamic crossover and, more importantly, the activated dynamics associated with bond breaking do not universally scale with interaction potential parameters in the same manner as do the equilibrium spinodal demixing and percolation boundaries. The conflicting experimental conclusions concerning whether kinetic gelation of sticky spherical particle suspensions can occur in a homogeneous phase are suggested to be a consequence of these theoretical considerations. Homogeneous phase gelation of spherical particle gels is predicted to be possible, consistent with silica nanoparticle experiments.[45–47]

Achieving kinetic arrest in the one-phase region becomes generically easier as colloids elongate. Rod phase separation occurs in a similar region of parameter space as for spheres of matched diameter and chemistry. This relative insensitivity results in an enhanced ability to achieve a kinetically stable, space-spanning gel in the homogeneous phase for more elongated particles.

We have also studied the relationship between kinetic arrest and percolation in one component nanorod and nanosphere fluids. Percolation is very sensitive to attraction strength and range, and can occur before or after the dynamic crossover transition that signals physical bonding and cluster formation. If the dynamic crossover occurs before percolation, one expects only microscopic clusters. Realization of such a kinetic state is easier with shorter range attractions. Another key parameter that controls percolation relative to gelation is the rod aspect ratio. Longer rods more readily kinetically arrest and percolate in the homogeneous fluid phase.

Connectivity percolation in rod-sphere mixtures is found to depend strongly on aspect ratio, attraction strength, and attraction range. The mixture percolation threshold varies almost linearly with attraction strength for $\beta\varepsilon$ in the range of 0–3. As expected, percolation is enhanced by the addition of rods to athermal and attractive sphere fluids. For pure rod or sphere fluids, the number of sticky contacts is roughly constant along the connectivity percolation threshold boundary, in agreement with a heuristic formulation of percolation where the threshold is *assumed* to be determined by the formation of a critical number of bonded neighbors.[43]

Ongoing and future work is proceeding in several directions. First, the question of kinetic arrest and novel dynamical states in chemically matched mixtures of rods and spheres is an interesting problem.[58] The elasticity and stress-driven yielding of such mixtures is of both scientific and materials engineering importance. Second, we are interested in learning the design rules for simultaneously optimizing the linear and nonlinear mechanical properties, and electrical conductivity, in metallic mixtures of rod and sphere nanoparticles for applications in direct write printing of conductive gel inks.[4] Clearly, the formation of space spanning, kinetically arrested, rigid, conductive gels will be aided by the addition of anisotropic rods, if macrophase separation is avoided. Finally, how the above questions and phenomena change if the matched chemistry condition is relaxed, energetically and/or sterically, is an open area of high interest.

ACKNOWLEDGMENTS

We thank Professor Jennifer Lewis and Professor Chip Zukoski for helpful and stimulating discussions. This work was supported by DOE-BES under Grant No. DE-FG02-07ER46471 administered through the Frederick Seitz Materials Research Laboratory.

[1] W. B. Russel, D. A. Saville, and W. R. Schowalter, *Colloidal Dispersions* (Cambridge University Press, New York, 1999).
[2] R. G. Larson, *The Structure and Rheology of Complex Fluids* (Oxford University Press, New York, 1999).
[3] J. A. Lewis, J. Am. Ceram. Soc. **83**, 2341 (2000).
[4] B. Y. Ahn, E. B. Duoss, M. J. Motala, X. Guo, S. I. Park, Y. Xiong, J. Yoon, R. G. Nuzzo, J. A. Rogers, and J. A. Lewis, Science, **323** 1590 (2009).
[5] J. M. Ziman, *Models of Disorder* (Cambridge University Press, New York, 1979).
[6] D. Stauffer and A. Aharony, *Introduction to Percolation Theory* (CRC, Philadelphia, 1994).
[7] M. Lupkowski and P. A. Monson, J. Chem. Phys. **89**, 8300 (1988).
[8] A. Coniglio, U. De Angelis, A. Forlani, and G. Lauro, J. Phys. A: Math. Gen. **10**, 219 (1977).
[9] A. Coniglio, U. De Angelis, and A. Forlani, J. Phys. A: Math. Gen. **10**, 1123 (1977).
[10] Y. C. Chiew and E. D. Glandt, J. Phys. A: Math. Gen. **16**, 2599 (1983).
[11] Y. C. Chiew, J. Chem. Phys. **110**, 10482 (1999).
[12] T. Simone, S. Demoulini, and R. M. Stratt, J. Chem. Phys. **85**, 391 (1986).
[13] X. Wang and A. P. Chatterjee, J. Chem. Phys. **116**, 347 (2002).
[14] A. P. Chatterjee, J. Chem. Phys. **117**, 10888 (2002).
[15] A. P. Chatterjee, J. Chem. Phys. **132**, 224905 (2010).
[16] K. Leung and D. Chandler, J. Stat. Phys. **63**, 837 (1991).
[17] K. S. Schweizer and J. G. Curro, Adv. Polym. Sci. **116**, 319 (1993).
[18] J. P. Hansen and I. R. McDonald, *Theory of Simple Liquids*, 2nd ed. (Academic Press, London, 1986).
[19] W. Gotze, J. Phys. Condens. Matter, **11**, A1 (1999); W. Götze and L. Sjörgen, Rep. Prog. Phys. **55**, 241 (1992).
[20] E. J. Saltzman and K. S. Schweizer, J. Chem. Phys. **119**, 1181 (2003); K. S. Schweizer, J. Chem. Phys. **123**, 244501 (2005).
[21] K. S. Schweizer, Curr. Opin. Colloid Interface Sci. **12**, 297 (2007).
[22] G. Yatsenko and K. S. Schweizer, Phys. Rev. E **76**, 014506 (2007); J. Chem. Phys. **126**, 014505 (2007).
[23] M. Tripathy and K. S. Schweizer, Phys. Rev. E **83**, 041407 (2011); Phys. Rev. E **83**, 041406 (2011).
[24] R. Zhang and K. S. Schweizer, Phys. Rev. E **80**, 011502 (2009); J. Chem. Phys. **133**, 104902 (2010).
[25] E. Zaccarelli, J. Phys. Condens. Matter **19**, 323 (2007).
[26] F. Sciortino, Nat. Mater., **1**, 145 (2002).
[27] K. Dawson, Curr. Opin. Colloid Interface Sci. **7**, 2187 (2002).
[28] J. Bergenholtz and M. Fuchs, Phys. Rev. E **59**, 5706 (1999); L. Fabbian, W. Gotze, F. Sciortino, P. Tartaglia, and F. Thiery, *ibid.* **59**, R1347 (1999); K. Dawson, G. Foffi, M. Fuchs, W. Götze, F. Sciortino, M. Sperl, P. Tartaglia, Th. Voigtmann, and E. Zaccarelli, Phys. Rev. E **63**, 011401 (2000).

[29]K. N. Pham, A. M. Puertas, J. Bergenholtz, S. U. Egelhaaf, A. Moussaïd, P. N. Pusey, A. B. Schofield, M. E. Cates, M. Fuchs, and W. C. K. Poon, Science **296**, 104 (2002).
[30]Y. L. Chen and K. S. Schweizer, J. Chem. Phys. **120**, 7212 (2004).
[31]Y. L. Chen, V. Kobelev, and K. S. Schweizer, Phys. Rev. E **71**, 041405 (2005).
[32]P. Lu, E. Zaccarelli, F. Ciulla, A. B. Schofield, F. Sciortino, and D. A. Weitz, Nat. Lett. **453**, 499 (2008).
[33]J. J. Adams, E. J. Duoss, T. Malkowski, M. Motala, B. Y. Ahn, R. G. Nuzzo, J. T. Bernhard, and J. A. Lewis, Adv. Mater. **23**, 1304 (2011).
[34]D. Chandler and H. C. Andersen, J. Chem. Phys. **57**, 1930 (1972).
[35]T. R. Kirkpatrick and P. G. Wolynes, Phys. Rev. A **35**, 3072 (1987).
[36]R. C. Kramb, R. Zhang, K. S. Schweizer, and C. F. Zukoski, Phys. Rev. Lett. **105**, 055702 (2010).
[37]R. Zhang and K. S. Schweizer, Phys. Rev. E **83**, 060502(R) (2011).
[38]H. A. Kramers, Physica (Amsterdam) **7**, 284 (1940).
[39]D. C. Viehman and K. S. Schweizer, Phys. Rev. E **78**, 051404 (2008); J. Chem. Phys. **128**, 084509 (2008).
[40]M. Doi and S. F. Edwards, *The Theory of Polymer Dynamics* (Oxford University Press, New York, 1986).
[41]L. Onsager, Ann. N. Y. Acad. Sci. **51**, 627 (1949).
[42]M. J. Solomon and P. T. Spicer, Soft Matter **6**, 1391 (2010).
[43]U. Alon, I. Balberg, and A. Drory, Phys. Rev. Lett. **66**, 2879 (1991).
[44]A. L. Bug, S. A. Safran, G. S. Grest, and I. Webman, Phys. Rev. Lett. **55**, 1896 (1985).
[45]A. P. R. Eberle, N. J. Wagner, and R. Castañeda-Priego, Phys. Rev. Lett. **106**, 105704 (2011).
[46]A. Shah, Y. L. Chen, K. S. Schweizer, and C. F. Zukoski, J. Chem. Phys. **119**, 8747 (2003); S. Ramakrishnan, Y. L. Chen, K. S. Schweizer, and C. F. Zukoski, Phys. Rev. E **70**, 040401(R) (2004); A. Shah, S. Ramakrishnan, Y. L. Chen, K. S. Schweizer, and C. F. Zukoski, J. Phys. Condens. Matter **15**, 4751 (2003).
[47]S. Ramakrishnan, V. Gopalakrishnan, and C. F. Zukoski, Langmuir **21**, 9917 (2005).
[48]E. R. Weeks and D. A. Weitz, Chem. Phys. **284**, 361 (2002); W. Kegel and A. vanBlaaderen, Science **287**, 290 (2000).
[49]G. Foffi, C. DeMichele, F. Sciortino and P. Tartaglia, Phys. Rev. Lett. **94**, 078301 (2005).
[50]M. A. Miller and D. Frenkel, Phys. Rev. Lett. **90**, 135702 (2003).
[51]M. G. Noro and D. Frenkel, J. Chem. Phys. **113**, 2941 (2000).
[52]D. L. Pagan and J. D. Gunton, J. Chem. Phys. **122**, 184515 (2005).
[53]M. A. Miller and D. Frenkel, J. Chem. Phys. **121**, 535 (2004).
[54]J. Bergenholtz and M. Fuchs, J. Phys. Condens. Matter **11**, 10171 (2000).
[55]J. Bergenholtz, M. Fuchs, and Th. Voightmann, J. Phys. Condens. Matter **12**, 6575 (2000); J. Bergenholtz, M. Fuchs, and W. C. K. Poon, Langmuir **19**, 4493 (2003).
[56]P. J. Flory, J. Chem. Phys. **10**, 51 (1942).
[57]G. Yatsenko and K. S. Schweizer, Langmuir **24**, 7474 (2008).
[58]R. Jadrich and K. S. Schweizer (unpublished).